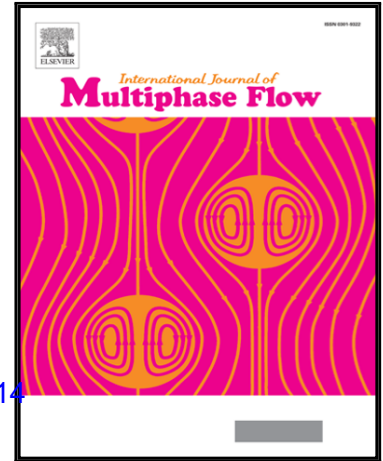


Accepted Manuscript

Inhomogeneity and anisotropy in Eulerian-Eulerian near-wall modelling

M. Riella, R. Kahraman, G.R. Tabor

PII: S0301-9322(18)30493-2
DOI: <https://doi.org/10.1016/j.ijmultiphaseflow.2019.01.014>
Reference: IJMF 2963



To appear in: *International Journal of Multiphase Flow*

Received date: 10 July 2018
Revised date: 16 December 2018
Accepted date: 31 January 2019

Please cite this article as: M. Riella, R. Kahraman, G.R. Tabor, Inhomogeneity and anisotropy in Eulerian-Eulerian near-wall modelling, *International Journal of Multiphase Flow* (2019), doi: <https://doi.org/10.1016/j.ijmultiphaseflow.2019.01.014>

This is a PDF file of an unedited manuscript that has been accepted for publication. As a service to our customers we are providing this early version of the manuscript. The manuscript will undergo copyediting, typesetting, and review of the resulting proof before it is published in its final form. Please note that during the production process errors may be discovered which could affect the content, and all legal disclaimers that apply to the journal pertain.

Highlights

- A pressure-velocity model to account for the no permeability constraint is proposed for E-E simulations.
- The model is derived within a Reynolds-Averaged Two-Fluid model framework and implemented within the open-source CFD toolbox OpenFOAM.
- The approach is capable of accounting for the strong near-wall inhomogeneity, a flow feature that hitherto has been neglected in Eulerian-Eulerian modelling.
- The predictions reveal that the approach proposed herein can lead to a satisfactory agreement across all turbulence statistics paving the way for the correct prediction of more complex mechanisms.
- The source code of the recently developed solver `ratfmFoam` and supplementary material used in this work is made available online.

Inhomogeneity and anisotropy in Eulerian-Eulerian near-wall modelling

M. Riella^{a,*}, R. Kahraman^b, G. R. Tabor^a

^a*College of Engineering, Mathematics and Physical Sciences, University of Exeter, North Park Road, Exeter EX4 4QF, UK*

^b*HiETA Technologies Ltd, Bristol & Bath Science Park, Dirac Crescent, Emersons Green, Bristol, BS16 7FR, UK*

Abstract

This paper tackles the issue of image vorticity in turbulent Eulerian-Eulerian simulations. A pressure-velocity model to account for the no permeability constraint on the fluid- and particle-phase wall normal stress components is proposed. The pressure-velocity model is derived within a Reynolds-Averaged Two-Fluid model (RA-TFM) framework and is implemented within the open-source CFD toolbox OpenFOAM. We demonstrate that this approach is capable of accounting for the strong near-wall inhomogeneity, a flow feature that hitherto has been neglected in Eulerian-Eulerian modelling. Simulation predictions are validated against benchmark Direct Numerical Simulation data and show a promising step forward in near-wall modelling in Eulerian-Eulerian simulations. The predictions reveal that the approach proposed herein can lead to a satisfactory agreement across all turbulence statistics paving the way for the correct prediction of more complex mechanisms. Finally, the source code of the recently developed solver `ratfmFoam` and supplementary material used in this work is made available online.

Keywords: RA-TFM, Near-wall, Eulerian-Eulerian, v2f, turbulence

*Corresponding author

Email address: `mjr214@exeter.ac.uk` (M. Riella)

1 1. Introduction

2 The near-wall behaviour of particle-laden fluid behaviour has been a challenging
3 topic for researchers over the preceding decades. Modelling the highly inhomoge-
4 neous near-wall region in a turbulent shear flow has proved difficult even in single
5 phase flows [1]. One phenomenon in particular that has proven challenging is the so-
6 called image vorticity [2, 3] that is caused by the kinematic blocking by the wall. This
7 non-local effect on the Reynolds stress arises due to the physical inviscid boundary
8 condition i.e. the no-flux condition on the normal component of velocity $\mathbf{u} \cdot \mathbf{n} = 0$.
9 This effect results in a highly anisotropic distribution amongst the Reynolds stress
10 components in the vicinity of a wall, mainly it is felt as a suppression of energy
11 transfer into the wall-normal component.

12 To circumvent these issues Durbin [4] proposed a pressure-velocity model based on
13 the Reynolds-Stress wall-normal component and an elliptical relaxation function to
14 account for the kinematic blocking effect. In single-phase simulations this approach
15 has proven fruitful [5, 6, 4, 7, 8, 9], with results showing distinct improvements over
16 simulations with damping-functions and in particular wall-functions, as neither can
17 account for the so-called stagnation-point anomaly or imposed pressure gradients.

18 Owing largely to its maturity and complexity, research in turbulent near-wall
19 fluid-particle modelling in an Eulerian-Eulerian (E-E) framework has been sparse.
20 One notably study is that of Rizk and Elghobashi [10] in which a theoretical study
21 was carried out to ascertain the effects of increasing volume fraction on the mean
22 velocity profile. They found that the log-layer broke down in their model speculating
23 that a standard wall-function may not be representative of particle-laden flow. This
24 postulation was somewhat corroborated by Vreman et al. [11] who showed that the
25 log-layer was retained but resulted in an adjustment of the von Karman “constant”.
26 In addition to this, Benyahia et al. [12] showed that the effect of the particle phase
27 could be included in the wall-function in an ad-hoc manner which allows the par-
28 ticle phase to influence the fluid phase velocity when the particle-fluid co-variance
29 remained correlated.

30 The use of single-phase wall functions in E-E simulations are abundant in litera-
31 ture [13, 14, 15, 16, 17]. The wall functions are applied to the fluid phase regardless
32 of the volume fraction in which complicated one- or two-way coupling effects can
33 play a role. Moreover, the universal form of the log-layer neglects pressure gradients,
34 with the addition of particles an induced hydro-static pressure gradient can com-
35 monly be found in the boundary layer. Attempts to circumvent this issue through
36 damping functions have been used [18, 19, 10, 20]. This introduces further complica-
37 tions with arbitrarily matching experimental/Direct Numerical Simulation (DNS) in
38 new or more complicated geometries. The drawbacks of damping-functions are well

39 known i.e. their arbitrariness and dampening the incorrect scale [21].

40 In the literature E-E simulations in the near-wall region rarely predict the correct
 41 turbulence statistics in the particle phase. Moreover, the particle-phase wall normal
 42 component can not be correctly predicted due to the $k - \varepsilon$ modelling assumptions
 43 i.e. the eddy-viscosity approximation for the pressure-velocity redistribution terms.
 44 In the particle phase this is particularly problematic as the wall-normal component
 45 is known to govern segregation towards the wall [22, 23] and can inhibit the correct
 46 volume fraction distribution.

47 A more fundamental explanation can be given when considering E-E (Two-Fluid
 48 Models) models. In the current E-E the correlated fluctuating component of the par-
 49 ticle phase is equated to the uncorrelated fluctuating energy of the particle phase.
 50 This error was first elucidated by Fevrier et al. [24] in which the partitioning effect of
 51 particle inertia was shown to give rise to two different contributions to the particle
 52 phase energy, namely correlated and uncorrelated energy. This distinction is crucial
 53 in both collisional and non-collisional flow Fox [25], Fevrier et al. [24] and has been
 54 shown to predict the correct physics in comparison with the current E-E models in
 55 which the distinction is not made Riella et al. [26].

56 In the near-wall region this distinction can prove particularly crucial. As the
 57 Stokes number, St increases as the wall is approached the correlated particle-phase
 58 energy k_p is dissipated into uncorrelated particle-phase energy Θ_p . This Stokes de-
 59 pendent behaviour is vital to predicting the correct distribution of particle-phase
 60 energy in the near-wall region. Without accounting for this behaviour, in combina-
 61 tion with wall-functions or damping functions it is clear why the near-wall region has
 62 proven particularly challenging and has received little attention Peirano and Leckner
 63 [27].

64 Within the context of near-wall modelling the turbulence constants may need to
 65 be changed to account for the presence of the particles. Bolio et al. [18] reported
 66 no significant changes in C_1 , C_2 , σ_k and σ_ε . Despite this Fox [25] has shown that
 67 there in-fact is a small dependence on the Stokes number for homogeneous-shear flow
 68 - change in C_2 . In the near-wall region the picture is complicated further and no
 69 experimental or DNS data exists. In this study we do not consider the influence of
 70 the turbulence constants but it is recognised here that with increased mass loading
 71 and Stokes number the constants may need to be changed. Within the near-wall
 72 region this is particularly uncertain and more research needs to be done.

73 In this paper we propose a pressure-velocity model in both phases. Within the
 74 E-E framework we assume continuous inter-penetrating phenomena and both phases
 75 share their pressure field. Recognising this is crucial for justifying the modelling
 76 decisions. We propose that the pressure reflection caused by the wall is felt in both

77 phases and as a result we can derive a pressure-velocity model for each phase. The
78 suppression of the wall-normal component enters the Reynolds stress transport equa-
79 tion through the velocity-pressure gradient correlation and is a term that appears in
80 the Reynolds stress equation for both phases.

81 To investigate the applicability of the model we apply it to a benchmark channel
82 flow case. The pressure-velocity model is derived and applied with a Reynolds-
83 Averaged Two-Fluid Model framework [25, 26]. Predictions are compared against
84 the Direct-Numerical-Simulation data of Marchioli and colleagues [28]. Two cases
85 are simulated with increasing Stokes number to highlight the partitioning effect of
86 particle inertia. Additionally, a mesh independence study is carried out, due to
87 the necessary resolution of the mesh to resolve the boundary layer, to ascertain the
88 sensitivity of the models predictions.

89 2. Numerical Model

90 The RA-TFM governing equations along with the recently derived multiphase
 91 $\overline{v_f^2} - f$ model [29] can be found in Table 1. The derivation of which can be found
 92 in Appendix A. Due to flow regime under consideration the buoyancy induced terms
 93 are neglected throughout this work. For a thorough description of the model the
 94 reader is referred to Fox [25]. The reader should note that the variables presented
 95 herein are the Phase-Averaged (PA) variables and their definitions can be found in
 96 Table 5.

97 The particle phase turbulent kinetic energy transport equation reads:

$$98 \quad \frac{\partial(\alpha_p \rho_p k_p)}{\partial t} + \nabla \cdot (\alpha_p \rho_p k_p \mathbf{u}_p) = \nabla \cdot \left(\mu_p + \frac{\mu_{pt}}{\sigma_{pk}} \right) \nabla k_p + \alpha_p \rho_p \Pi_p - \alpha_p \rho_p \varepsilon_p \quad (1)$$

$$+ 2\beta(k_{fp} - k_p)$$

99 The first term on the RHS is the particle phase turbulent kinetic dissipation
 100 energy flux. The second term Π_p is kinetic energy production due to mean shear
 101 with the third term being its dissipation. The remaining term is the coupling terms
 102 due to velocity correlations. The coupling terms take the form of $k_{fp} = \sqrt{k_f k_p}$ and
 103 $\varepsilon_{fp} = \sqrt{\varepsilon_f \varepsilon_p}$. These terms represent the fluid-velocity covariance. The particle phase
 104 turbulent kinetic energy dissipation transport equation reads:

$$\frac{\partial(\alpha_p \rho_p \varepsilon_p)}{\partial t} + \nabla \cdot (\alpha_p \rho_p \varepsilon_p \mathbf{u}_p) = \nabla \cdot \left(\mu_p + \frac{\mu_{pt}}{\sigma_{pk}} \right) \nabla \varepsilon_p + \frac{\varepsilon_p}{k_p} (C_{\varepsilon 1} \alpha_p \rho_p \Pi_p - C_{\varepsilon 2} \alpha_p \rho_p \varepsilon_p)$$

$$+ 2\beta(\varepsilon_{fp} - \varepsilon_p) \quad (2)$$

105 The first term on the RHS is the particle phase turbulent kinetic dissipation
 106 energy flux. The second term Π_p is kinetic energy production due to mean shear
 107 with the third term being its dissipation. The remaining term is the coupling term
 108 due to velocity correlations. The granular temperature transport equation reads:

$$\frac{3}{2} \left[\frac{\partial(\alpha_p \rho_p \Theta_p)}{\partial t} + \nabla \cdot (\alpha_p \rho_p \Theta_p \mathbf{u}_p) \right] = \nabla \cdot \left(\kappa_{\Theta} + \frac{3\mu_{pt}}{2Pr_{pt}} \right) \nabla \Theta_p + 2\mu_p \overline{\mathbf{S}}_p : \overline{\mathbf{S}}_p \quad (3)$$

$$- p_p \nabla \cdot \mathbf{u}_p + \alpha_p \rho_p \varepsilon_p - 3\beta \Theta_p - \gamma$$

109 The first term on the RHS is the PA granular temperature flux which is made
 110 up of two contributions, the granular temperature flux and the turbulent granular
 111 flux. The former is the granular conductivity of which there are various formulations
 112 in the literature. Here the formulation of Syamlal and O'Brien [30] is used as it
 113 correctly tends to zero in the dilute limit [31]. The latter term is the turbulent flux

114 and includes the particle turbulent viscosity. The second term is a laminar source
 115 term due to viscous stresses. The third term is a pressure dilation term which ac-
 116 counts for compressibility. The fourth term is of particular interest as it represents
 117 the turbulent particle kinetic energy dissipation which appears here as a positive
 118 source term. The physical interpretation of this means that as large scale particle
 119 turbulent kinetic energy is dissipated, small scale granular temperature is produced.
 120 The two remaining terms represent decrease of granular temperature due to drag
 121 and decrease of granular temperature due to inelastic collisions.

122

123 2.1. Derivation of particle-phase pressure-velocity model

124 In order to derive the transport equation for the particle-phase wall normal com-
 125 ponent one needs to begin at the exact RA Reynolds stress transport equation. It
 126 can be found by Reynolds-Averaging the PA velocity tensor transport equation and
 127 subtracting the PA particle-phase mean velocity tensor transport equation. A rigor-
 128 ous derivation can be found in [32] and for the sake of brevity will not be presented
 129 here.

$$\begin{aligned}
 & \frac{\partial \langle \alpha_p \rangle \langle \mathbf{u}_p'' \otimes \mathbf{u}_p'' \rangle_p}{\partial t} + \nabla \cdot \langle \alpha_p \rangle \langle \mathbf{u}_p \rangle_p \otimes \langle \mathbf{u}_p'' \otimes \mathbf{u}_p'' \rangle_p = -\nabla \cdot \langle \alpha_p \rangle \langle \mathbf{u}_p'' \otimes \mathbf{u}_p'' \otimes \mathbf{u}_p'' \rangle_p \\
 & \quad - \underbrace{\langle \alpha_p \rangle \langle \langle \mathbf{u}_p'' \otimes \mathbf{u}_p'' \rangle_p \cdot \nabla \langle \mathbf{u}_p \rangle_p \rangle}_{\text{Production}} + \frac{1}{\rho_p} \nabla \cdot \langle \bar{\boldsymbol{\sigma}}_p \otimes \mathbf{u}_p'' \rangle - \frac{1}{\rho_p} \nabla \langle p_p \mathbf{u}_p'' \rangle \\
 & + \underbrace{\frac{1}{\rho_p} \langle p_p \nabla \mathbf{u}_p'' \rangle}_{\text{pressure strain, } \phi_{p,yy}} - \underbrace{\frac{1}{\rho_p} \langle \bar{\boldsymbol{\sigma}}_p \cdot \nabla \mathbf{u}_p'' \rangle}_{\text{dissipation, } \varepsilon_{p,yy}} + \underbrace{\langle \alpha_p \rangle \beta \langle \langle \mathbf{u}_f''' \otimes \mathbf{u}_p'' \rangle_p - \langle \mathbf{u}_p'' \otimes \mathbf{u}_p'' \rangle_p \rangle}_{\text{velocity correlations}}
 \end{aligned} \tag{4}$$

130 We postulate that an imaginary particle phase wall normal component transport
 131 equation can be derived with adequate closure to the terms presented in Eq. 4.
 132 Firstly, we recognise that the production term is a function of the mean flow gradients
 133 in the stream-wise direction therefore it is dropped.

134 The velocity correlations which arise due to phase coupling are dominant in this
 135 work and have been shown to display the correct behaviour in one-way coupled
 136 flow Fox [25]. We therefore adopt the same form for their closure by setting the
 137 co-variance of the fluctuations $\langle \mathbf{u}_f''' \otimes \mathbf{u}_p'' \rangle_p = \overline{v_{fp}^2} = \sqrt{v_p^2 v_f^2}$.

138 Following the standard approach used in classic eddy-viscosity turbulence models,
 139 the divergence terms appearing in the transport equation are closed by the eddy-

140 diffusivity approximation [1].

$$\nabla \cdot \left[\frac{\mu_{pt}}{\sigma_{pk}} \nabla \langle \mathbf{u}_p'' \otimes \mathbf{u}_p'' \rangle_p \right] \approx -\nabla \cdot \langle \alpha_p \rangle \langle \mathbf{u}_p'' \otimes \mathbf{u}_p'' \otimes \mathbf{u}_p'' \rangle_p + \frac{1}{\rho_p} \nabla \cdot \langle \bar{\boldsymbol{\sigma}}_p \otimes \mathbf{u}_p'' \rangle - \frac{1}{\rho_p} \nabla \langle p_p \mathbf{u}_p'' \rangle \quad (5)$$

141 Finally, the terms left to close are the pressure strain and dissipation terms. These
142 terms are explicitly modelled in the $\overline{v_p^2} - f$ transport equation and are grouped into
143 a source term denoted $k_p f$.

$$k_p f = \underbrace{\phi_{p,yy}}_{\text{pressure strain}} - \underbrace{\varepsilon_{p,yy}}_{\text{dissipation}} + \alpha_p \rho_p 6 \frac{\overline{v_p^2}}{k_p} \varepsilon_p \quad (6)$$

144 The source term effectively redistributes turbulence energy from the stream-wise
145 Reynolds stress component to the wall-normal component close to walls. This means
146 that particle turbulence energy can only enter the wall-normal component through
147 redistribution. The source term has been shown to overproduce in regions relatively
148 far away from the wall and the correction of Davidson et al. [6] is employed.

$$\overline{v_{p,source}^2} = \min \left\{ k_p f, -\frac{1}{T} \left[(C_1 - 6) \overline{v_p^2} - \frac{2k_p}{3} (C_1 - 1) \right] + C_2 \Pi_p \right\} \quad (7)$$

149 Now setting the wall-normal component of the fluid-phase Reynolds stress tensor
150 $\langle \mathbf{u}_p'' \otimes \mathbf{u}_p'' \rangle_p$ to $\overline{v_p^2}$ a transport equation can be written as:

$$\frac{\partial(\alpha_p \rho_p \overline{v_p^2})}{\partial t} + \nabla \cdot (\alpha_p \rho_p \overline{v_p^2} \mathbf{u}_p) = \nabla \cdot \left(\mu_p + \frac{\mu_{pt}}{\sigma_{pk}} \right) \nabla \overline{v_p^2} + \alpha_p \rho_p \overline{v_{p,source}^2} - \alpha_p \rho_p 6 \frac{\overline{v_p^2}}{k_p} \varepsilon_p + 2\beta(\overline{v_{fp}^2} - \overline{v_p^2}) \quad (8)$$

151 The reader should note that the third term is a sink term that is used to balance
152 the source term $k_p f$. This is a modification proposed by Lien and Kalitzin [8] and
153 ensures that the source term $k_p f \rightarrow 0$ as it approaches the wall.
154

155 Eq. 8 contains no sensitivity to the wall distance and thus a modified Helmholtz
156 equation is constructed to form an elliptic relaxation equation. The form of this
157 equation accounts for anisotropy close to walls and is also independent of Reynolds

158 number and y^+ value which reads

$$L_p^2 \frac{\partial^2 f}{\partial x^2} - f = \underbrace{\frac{C_1}{T_p} \left(\frac{\overline{v_p^2}}{k_p} - \frac{2}{3} \right)}_{\phi_{p,yy,S}} - \underbrace{C_2 \frac{\Pi_p}{k_p}}_{\phi_{p,yy,R}} - \frac{1}{T_p} \left(6 \frac{\overline{v_p^2}}{k_p} - \frac{2}{3} \right) \quad (9)$$

159

160 The terms $\phi_{p,yy,S}$ and $\phi_{p,yy,R}$ are the so-called slow and rapid pressure-strain terms
 161 [33, 1] with the final term being used to ensure far field behaviour i.e. that the
 162 elliptic relaxation function diminishes away from walls. Solving a Poisson equation
 163 with a segregated solver can cause numerical issues due to its elliptical nature. This
 164 issue can be resolved by following Lien and Kalitzin [8] and introducing a sink and
 165 source term in $k_p f$ source term in the $\overline{v_p^2}$ and f transport equation of the form, $6 \frac{\overline{v_p^2}}{k_p}$.
 166 This enables a Dirichlet boundary condition to be prescribed. The eddy viscosity is
 167 calculated from the solution of the $\overline{v_p^2} - f$ model, again the correction proposed by
 168 Davidson et al. [6] is used.

$$\nu_{pt} = \min \left\{ C_{p\mu} k_p^2 / \varepsilon_p, C_\mu \overline{v_p^2} T_p \right\} \quad (10)$$

169

170 where the turbulent time and length scales are defined in analogy to those in the
 171 fluid phase, we can define a characteristic length and time scale based on the particle
 172 turbulent flow variables as:

$$T_p = \max \left(\frac{k_p}{\varepsilon_p}, 6 \sqrt{\frac{\nu_f}{\varepsilon_f}} \right) \quad (11)$$

$$L_p = \max \left(\frac{k_p^{3/2}}{\varepsilon_p}, C_\eta \frac{\nu_f^{3/4}}{\varepsilon_f^{1/4}} \right) \quad (12)$$

173

174 Both time and length scales are limited in regions close to the wall. In regions close
 175 to the wall k_p need not be zero but due to one-way coupling used in this work the
 176 mean slip $\rightarrow 0$ therefore the particles remain correlated. In regions close to the
 177 wall the particle characteristic time scale can reduce below the Kolmogorov scale
 178 hence limiting is applied. It is instructive to note that as the particle relaxation
 179 time increases closer to the wall and the particles become less responsive to the main
 180 flow uncorrelated energy Θ_p is created. Hence, at the correlated macro-scale k_p the
 181 production due to the velocity covariance is dominant but as the particle response

182 time increases uncorrelated meso-scale energy Θ_p is produced. As the fluid-particle
 183 flow remains correlated the scaling is retained.

184 2.2. Model setup and solution

185 The geometry comprises of two flat parallel walls. The computational domain
 186 of size $16\pi h \times 2h$, with x-, y- axes in the stream-wise and wall-normal directions,
 187 respectively. Four mesh resolutions are investigated with $y^+ = 0.5$ kept constant
 188 throughout with an inflation ratio of 1.1 in the y direction. For smaller y^+ values the
 189 computational cost increases dramatically due to the aspect-ratio and simulations
 190 become unfeasible.

191 The wall boundary condition for ε_f can be found in Table 3. For the remain-
 192 ing model variables the following boundary conditions at the wall are prescribed,
 193 $\mathbf{u}_f = k_f = \overline{v_f^2} = f = 0$. For the particulate phase a Neumann boundary condition is
 194 prescribed for the velocity and turbulence statistics. Both k_p and ε_p are initialised as
 195 1/3rd of their fluid counterpart with $\Theta_p = 1.0 \times 10^{-8} \text{m}^2 \text{s}^{-2}$. At the inlet a Dirichlet
 196 boundary condition is prescribed for both phase velocities and a Neumann condition
 197 for pressure. At the outlet a Dirichlet boundary condition is prescribed for pressure
 198 and a Neumann condition for both phase velocities.

199 The RA-TFM and the recently derived $\overline{v_p^2} - f$; $\overline{v_f^2} - f$ turbulence models are
 200 implemented into the open-source toolbox OpenFOAM [34]. The solver `ratfmFoam`
 201 is based on our previous work [26] and is made open-source. To handle the pressure-
 202 velocity coupling the Pressure Implicit with Splitting Operators (PISO) algorithm
 203 [35, 36] is used. The volume fraction is solved using Multi-dimensional Universal
 204 Limiter with Explicit Solution (MULES) [37] which is a flux-corrected transport al-
 205 gorithm which ensures robustness, stability and convergence. Time derivative terms
 206 are discretised using the first order accurate implicit Euler, gradients are discretised
 207 using the least squares scheme, convective terms are discretised using the second or-
 208 der central scheme (limitedLinearV/limitedLinear01). The former is used for vectors
 209 and the latter is used for bounding variables between 0 and 1. Finally, Laplacian
 210 schemes are discretised with the second order accurate central differencing scheme.

Table 1: Table of simulated cases

Case	d_p [μm]	ρ_p [kg/m^3]	St
1	20.4	1000	1
2	45.6	1000	5

Table 2: RA-TFM governing equations

Governing equations of the particle-phase:

$$\frac{\partial(\alpha_p \rho_p)}{\partial t} + \nabla \cdot (\alpha_p \rho_p \mathbf{u}_p) = 0 \quad (13)$$

$$\begin{aligned} \frac{\partial(\alpha_p \rho_p \mathbf{u}_p)}{\partial t} + \nabla \cdot (\alpha_p \rho_p \mathbf{u}_p \mathbf{u}_p) = \nabla \cdot 2(\mu_p + \mu_{pt}) \bar{\mathbf{S}}_p + \beta \left[(\mathbf{u}_f - \mathbf{u}_p) - \frac{\nu_{ft}}{\text{Sc}_{fs} \alpha_p \alpha_f} \nabla \alpha_p \right] \\ - \nabla p_p - \alpha_p \nabla p_f + \alpha_p \rho_p \left[1 - \alpha_f \left(1 - \frac{\rho_f}{\rho_p} \right) \right] \mathbf{g} \end{aligned} \quad (14)$$

Governing and phase-energy equations of the particle-phase:

$$\frac{\partial(\alpha_f \rho_f)}{\partial t} + \nabla \cdot (\alpha_f \rho_f \mathbf{u}_f) = 0 \quad (15)$$

$$\begin{aligned} \frac{\partial(\alpha_f \rho_f \mathbf{u}_f)}{\partial t} + \nabla \cdot (\alpha_f \rho_f \mathbf{u}_f \mathbf{u}_f) = \nabla \cdot 2(\mu_f + \mu_{ft}) \bar{\mathbf{S}}_f + \beta \left[(\mathbf{u}_p - \mathbf{u}_f) + \frac{\nu_{ft}}{\text{Sc}_{fs} \alpha_p \alpha_f} \nabla \alpha_p \right] \\ - \alpha_f \nabla p_f + \alpha_p \nabla p_f + \alpha_f \rho_f \left[1 + \alpha_p \left(\frac{\rho_p}{\rho_f} - 1 \right) \right] \mathbf{g} \end{aligned} \quad (16)$$

$$\begin{aligned} \frac{\partial(\alpha_f \rho_f k_f)}{\partial t} + \nabla \cdot (\alpha_f \rho_f k_f \mathbf{u}_f) = \nabla \cdot \left(\mu_t + \frac{\mu_{ft}}{\sigma_{fk}} \right) \nabla k_f + \alpha_f \rho_f \Pi_f - \alpha_f \rho_f \varepsilon_f \\ + 2\beta(k_{fp} - k_f) \end{aligned} \quad (17)$$

$$\begin{aligned} \frac{\partial(\alpha_f \rho_f \varepsilon_f)}{\partial t} + \nabla \cdot (\alpha_f \rho_f \varepsilon_f \mathbf{u}_f) = \nabla \cdot \left(\mu_t + \frac{\mu_{ft}}{\sigma_{fk}} \right) \nabla \varepsilon_f + \frac{\varepsilon_f}{k_f} \left[C_{\varepsilon 1} \alpha_f \rho_f \Pi_f - C_{\varepsilon 2} \alpha_f \rho_f \varepsilon_f \right] \\ + 2\beta(\varepsilon_{fp} - \varepsilon_f) \end{aligned} \quad (18)$$

$$\begin{aligned} \frac{\partial(\alpha_f \rho_f \overline{v_f^2})}{\partial t} + \nabla \cdot (\alpha_f \rho_f \overline{v_f^2} \mathbf{u}_f) = \nabla \cdot \left(\mu_f + \frac{\mu_{ft}}{\sigma_{fk}} \right) \nabla \overline{v_f^2} + \alpha_f \rho_f \overline{v_{f,source}^2} - \alpha_f \rho_f 6 \frac{\overline{v_f^2}}{k_f} \varepsilon_f \\ + 2\beta(\overline{v_{fp}^2} - \overline{v_f^2}) \end{aligned} \quad (19)$$

$$L^2 \frac{\partial^2 f}{\partial x^2} - f = \frac{C_1}{T} \left(\frac{\overline{v_f^2}}{k_f} - \frac{2}{3} \right) - C_2 \frac{\Pi_f}{k_f} - \frac{1}{T} \left(6 \frac{\overline{v_f^2}}{k_f} - \frac{2}{3} \right) \quad (20)$$

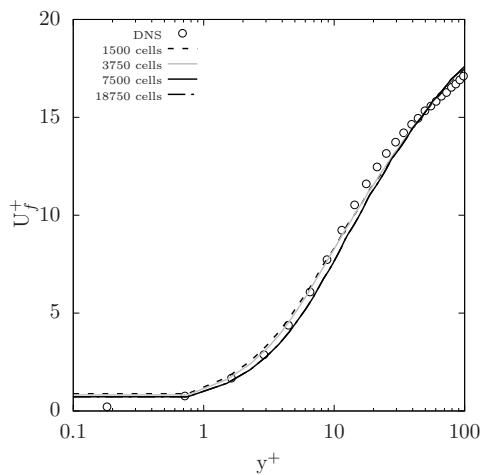
211 **3. Results and Discussion**212 *3.1. Influence of mesh resolution*

Figure 1: Mean fluid stream-wise velocity convergence

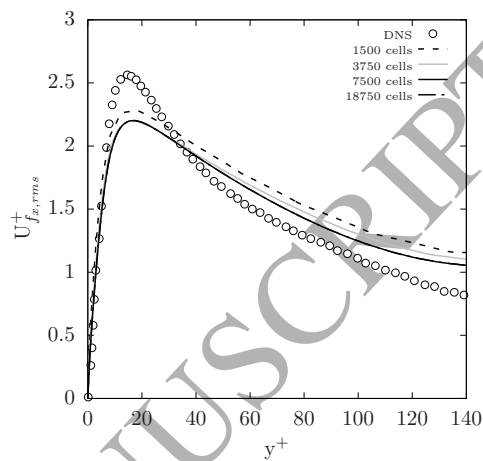


Figure 2: Fluid stream-wise fluctuation velocity convergence

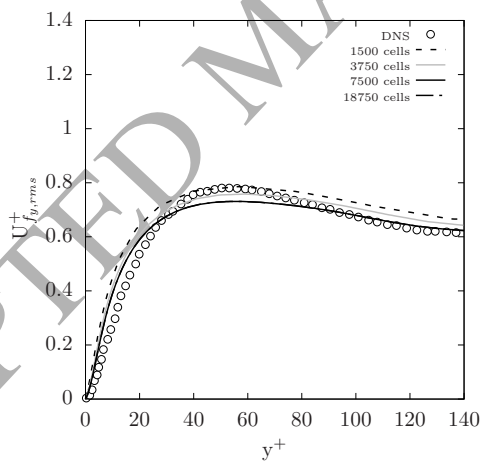


Figure 3: Fluid wall-normal fluctuation velocity convergence

213 To ascertain the influence of the mesh's resolution four different mesh sizes are
 214 compared; 1500, 3750, 7500 and 18750 cells pertaining to 25x50, 50x75, 75x100 and

215 1250x150 in the x- and y- direction, respectively. Simulations are run for 500s of
216 real flow time with all flow statistics being averaged through flow sampling. Flow
217 sampling takes place after 100s and is used to ascertain temporal sensitivity of the
218 solution. For the sake of brevity only the fluid flow statistics are shown here. Figs. [1-
219 3] show that with incremental increases in mesh resolution the results tend towards
220 a converged solution. The final two mesh resolutions reveal no change across all
221 three flow variables. These two mesh resolutions indicate that the solution is mesh
222 independent and no further enhancement of the resolution will change the solution.
223 For the sake of computational cost, and with no loss of accuracy, the former mesh
224 consisting of 7500 cells is used throughout this work.

225 3.2. Fluid phase

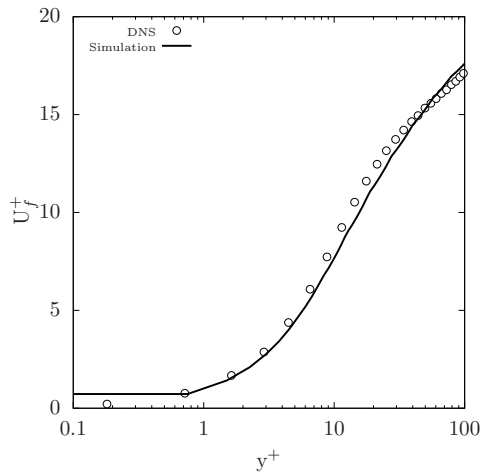


Figure 4: Mean fluid stream-wise velocity

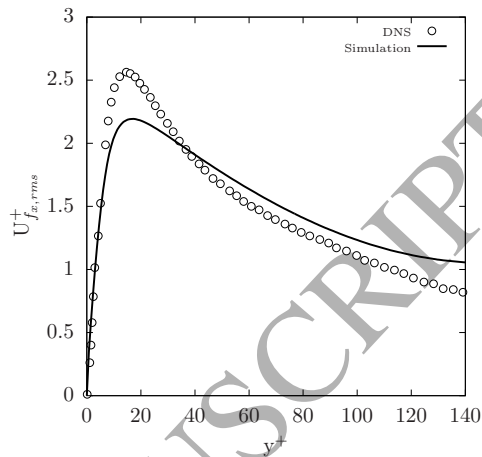


Figure 5: Fluid stream-wise fluctuation velocity

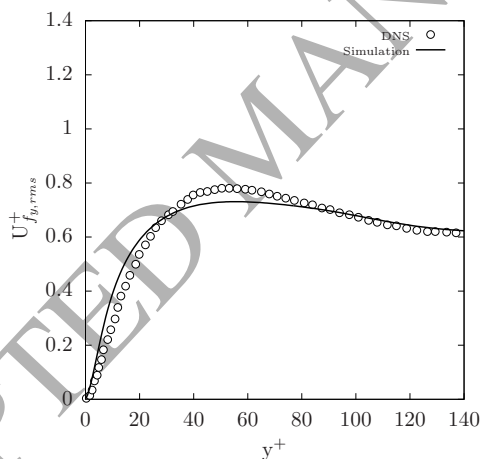


Figure 6: Fluid wall-normal fluctuation velocity

226 Fig. 4 shows the calculation of the mean fluid-phase velocity. There is a satis-
 227 factory prediction of the mean velocity spanning from the viscous wall region to the
 228 log-law region. This crucial region for predicting a number of phenomena i.e. heat
 229 transfer, particle-wall interaction and compressible flows can be accurately modelled
 230 with the $\overline{v}_f - f$ model. From $y^+ < 1$ there exists two mesh cells which explains the

231 perceived lack of gradient in this region, as mentioned in Section 2.2 a computational
232 limit is set for small values of y^+ , although the fluid-phase velocity components do
233 correctly tend to 0 as the wall is approached. It is an artifact of the lack of resolution
234 for very small values of y^+ and the logarithmic scaling.

235 In Fig. 5 the stream-wise fluctuation velocity is shown. Qualitatively the model
236 is in good agreement especially for an E-E simulation. Despite this two main dis-
237 crepancies can be seen: the under-prediction in the peak of fluid-phase turbulent
238 kinetic energy and the over-prediction of the turbulence decay in the free-stream.
239 Two explanations that perhaps feed into each other can be suggested. The first, if
240 one invokes continuity across the span of the channel it can be imagined that if the
241 production was increased the decay would increase. Thus we can postulate that if
242 the production was increased a larger peak would be displayed and as a result a
243 steeper gradient of decay would be shown.

244 The peak is governed by the production term, Π_f which is a function of the
245 fluid-phase turbulent viscosity and mean velocity gradients. The latter can be influ-
246 enced through numerical schemes - in particular the calculation of the gradient [35].
247 Secondly, due to the relatively small Reynolds number of the flow, $Re_\tau = 150$ the
248 turbulence model can fail to capture the correct turbulent kinetic energy behaviour.
249 This is due to the model being calibrated for high Reynolds number. In Durbin [4]
250 it is shown that for low Reynolds number flow the model over-predicts turbulence in
251 the free stream - a finding that is consistent with damping functions. It should be
252 noted that they also over-predicted the peak which was not the case in this study.
253 It would seem that an element of both are at work, therefore with calibrating of
254 the turbulence constants a more accurate fit could be obtained. It is also worth
255 mentioning that in the data of Marchioli et al. [28] the peak is the region in which
256 the greatest variance was reported. This is true of both phases and highlights the
257 difficulty in predicting a reliable value.

258 The near-wall behaviour of the wall-normal component has been accurately cap-
259 tured in Fig. 6. A slight underproduction is seen in the peak across the range
260 $40 < y^+ < 80$ which is expected as the value of the stream-wise fluctuating com-
261 ponent is also under-predicted. As discussed the wall-normal component receives
262 turbulent kinetic energy through redistribution - therefore the under-prediction is
263 experienced in both components. Overall excellent agreement with the DNS data is
264 found, this provides promising evidence for the application of the $v^2 - f$ model to
265 E-E modelling.

266 3.3. Particle phase statistics

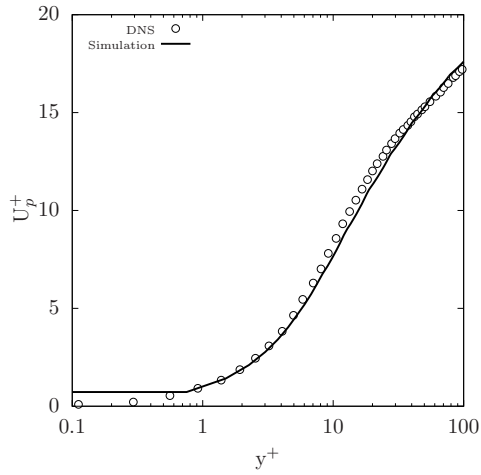


Figure 7: Mean particle stream-wise velocity, St = 1

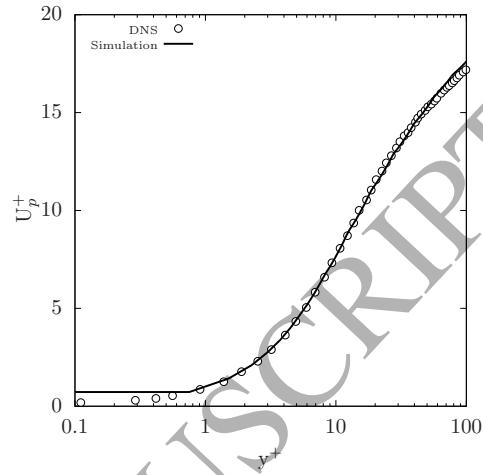


Figure 8: Mean particle stream-wise velocity, St = 5

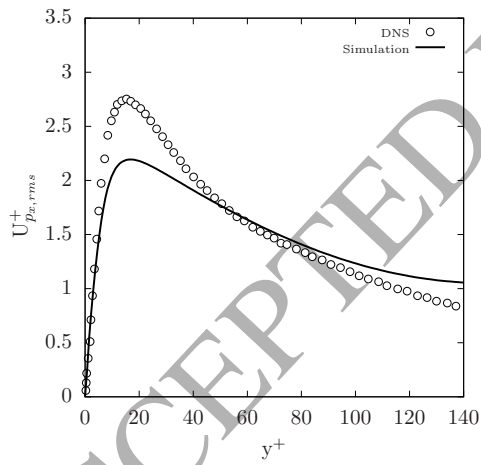


Figure 9: Particle stream-wise fluctuation velocity, St = 1

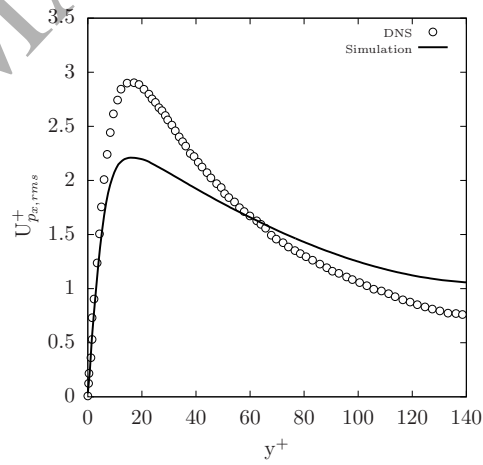


Figure 10: Particle stream-wise fluctuation velocity, St = 5

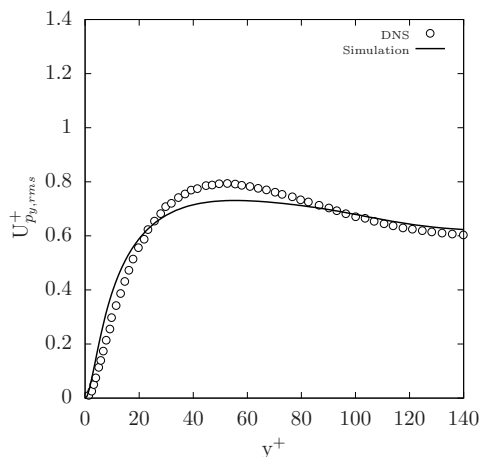


Figure 11: Particle wall-normal fluctuation velocity, $St = 1$

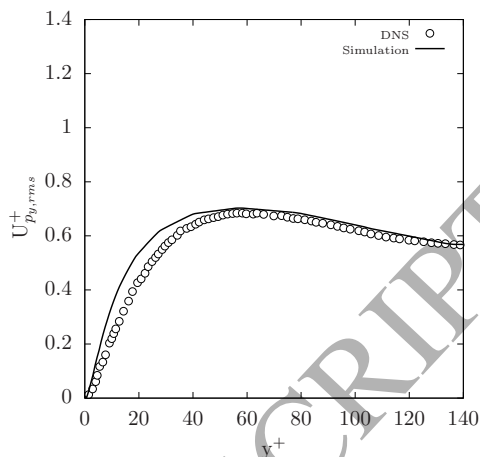


Figure 12: Particle wall-normal fluctuation velocity, $St = 5$

267 For the channel flow simulated in the work of Marchioli et al. [28] the fluid-particle
 268 co-variance terms dominate the particle-phase energy by providing the major con-
 269 tribution to their production via drag. As the particle phase is one-way coupled
 270 with the fluid phase the particles will be dragged along by the fluid and experience
 271 no feedback effect on the fluid phase. Even in such a flow it has been shown the
 272 need to partition the particle inertia into correlated and uncorrelated motion Fevrier
 273 et al. [24]. In the model used throughout this partitioning is denoted by k_p and Θ_p ,
 274 respectively.

275 Figs. 7-8 shows the prediction of the particle-phase mean velocity of which shows
 276 excellent agreement with the DNS data. The prediction of the mean velocity is well
 277 captured across the range of y^+ with the main discrepancy coming from the mesh
 278 resolution as discussed previously. Due to the close to non-existent slip velocity,
 279 owing to the geometry and governing physics, it is apparent that the von Neumann
 280 wall boundary condition results in the correct near-wall behaviour. Owing to the
 281 smoothness of the channel no effects due to roughness were incorporated, for further
 282 discussion the reader is referred to Vreman [38].

283 Figs. 9-10 reveal that the model is capable of capturing the Stokes dependent
 284 behaviour, which manifests itself in an increase in the peak of turbulent kinetic en-
 285 ergy, although the increase is not as large as that seen in the DNS. We recognise here
 286 that this increase of particle-phase turbulent kinetic energy is due to the increase in
 287 uncorrelated energy, Θ_p . As the particle response time increases the particles become
 288 uncorrelated with the main flow. This phenomenon has also been reported by Vance

289 et al. [39], Fevrier et al. [24] who showed that with increasing Stokes number an
 290 increasing fraction of the fluctuating energy was found in the random-uncorrelated
 291 motion, Θ_p .

292 We find that the increase in particle response time coupled with the dispersion
 293 enhances the "de-correlation" which is why the main increase is seen across $y^+ < 60$.
 294 The energy is re-partitioned into the near wall region showing an increase in the peak
 295 of the turbulent kinetic energy. As a result over the $y^+ > 60$ there is an increase
 296 in the gradient of turbulent kinetic energy decay, a feature that was not captured.
 297 It is interesting to note that this re-partitioning of the particle-phase energy is not
 298 especially felt in the mean-velocity profile.

299 In Fig. 10, even though an increase in the peak seen at $y^+ \approx 11.6$ is apparent the
 300 behaviour approaching the free-stream is at odds with the DNS data. The lack of
 301 turbulent kinetic energy decay is most apparent across $y^+ > 60$. It is clear that the
 302 distribution of the turbulence energy changes quite considerably with larger response
 303 times and a sharper gradient of decay is shown. This suggests that an adjustment
 304 of the the turbulent decay constant could be made a function of the particle Stokes
 305 number.

306 As shown in Marchioli and Soldati [40] preferential concentration is shown for
 307 Stokes number 5, a feature that was also seen in the simulation. We find in our
 308 simulations that with increasing particle response time particles tended to drift to-
 309 wards the wall becoming preferentially concentrated. A phenomenon that is well-
 310 established in the literature Reeks [22]. This behaviour was determined by the drift
 311 velocity as expected, which is a function the gradient of volume fraction and Stokes
 312 number. Figs. 11-12 show the particle-wall normal fluctuation velocity components.
 313 A satisfactory prediction across both simulations can be seen. The main discrepancy
 314 is the lack of peak in the former although the trend is captured elsewhere.

315 4. Conclusions

316 In this work we have presented a pressure-velocity model for both the particle-
 317 and fluid-phase for use in Eulerian-Eulerian simulations. The turbulence model was
 318 derived within a Reynolds-Averaged Two-Fluid Model framework and applied to
 319 channel flow. Throughout it has been shown that accounting for the kinematic
 320 blocking effect leads to promising results. Across both fluid and particle turbulence
 321 statistics a good agreement was shown, in particular the wall-normal energy compo-
 322 nent of each respective phase was well produced. A result that has hitherto alluded
 323 E-E simulations. The results were validated against benchmark Direct Numerical
 324 Simulation of Marchioli et al. [28] and show strong qualitatively and quantitatively

325 agreement. The RA-TFM shows the correct Stokes dependence behaviour exhibited
 326 in the particle-phase turbulence statistics. The current predictions show encouraging
 327 results and efforts should be made to extend the approach for more complex flow
 328 regimes i.e. two-way coupling.

329 5. Code repository

330 The source code of the `ratfmFoam` solver and supplementary material can be
 331 downloaded from [41] and is distributed under the terms of the GNU General Public
 332 License v3.

333 6. Acknowledgements

334 This work has benefited from a PhD Scholarship from the College of Engineering,
 335 Mathematics and Physical Sciences at the University of Exeter.

336 7. Appendix A

337 We begin with the exact RA Reynolds Stress transport equation for the fluid
 338 phase which is found by Reynolds-Averaging the PA velocity tensor transport equation
 339 and subtracting the PA fluid-phase mean velocity tensor transport equation.
 340 A rigorous derivation can be found in [32] and for the sake of brevity will not be
 341 presented here.

$$\begin{aligned}
 & \frac{\partial \langle \alpha_f \rangle \langle \mathbf{u}_f''' \otimes \mathbf{u}_f''' \rangle_f}{\partial t} + \nabla \cdot \langle \alpha_f \rangle \langle \mathbf{u}_f \rangle_f \otimes \langle \mathbf{u}_f''' \otimes \mathbf{u}_f''' \rangle_f = -\nabla \cdot \langle \alpha_f \rangle \langle \mathbf{u}_f''' \otimes \mathbf{u}_f''' \otimes \mathbf{u}_f''' \rangle_f \\
 & \quad - \underbrace{\langle \alpha_f \rangle \langle (\mathbf{u}_f''' \otimes \mathbf{u}_f''')_f \cdot \nabla \langle \mathbf{u}_f \rangle_f \rangle}_{\text{Production}} + \frac{1}{\rho_f} \nabla \cdot \langle \bar{\boldsymbol{\sigma}}_f \otimes \mathbf{u}_f''' \rangle - \frac{1}{\rho_f} \nabla \langle p_f \mathbf{u}_f''' \rangle \\
 & \quad + \underbrace{\frac{1}{\rho_f} \langle p_f \nabla \mathbf{u}_f''' \rangle}_{\text{pressure strain, } \phi_{f,yy}} - \underbrace{\frac{1}{\rho_f} \langle \bar{\boldsymbol{\sigma}}_f \cdot \nabla \mathbf{u}_f''' \rangle}_{\text{dissipation, } \varepsilon_{f,yy}} + \underbrace{\langle \alpha_f \rangle \beta \langle (\mathbf{u}_f''' \otimes \mathbf{u}_p'' - \langle \mathbf{u}_f''' \otimes \mathbf{u}_f''' \rangle_p) \rangle}_{\text{velocity correlations}}
 \end{aligned} \tag{21}$$

342 The velocity correlations which arise due to phase coupling are modelled analogously to those terms found in the $k_f - \varepsilon_f$ transport equations. We set the co-variance
 343 of the fluctuations $\langle \mathbf{u}_f''' \otimes \mathbf{u}_p'' \rangle_p = \overline{v_{fp}^2} = \sqrt{v_f^2 v_p^2}$. Following the standard approach used
 344

345 in classic eddy-viscosity turbulence models, the divergence terms appearing in the
346 transport equation are closed by the gradient-diffusion hypothesis [1].

$$\nabla \cdot \left[\frac{\mu_{ft}}{\sigma_{fk}} \nabla \langle \mathbf{u}_f''' \otimes \mathbf{u}_f''' \rangle_f \right] \approx -\nabla \cdot \langle \alpha_f \rangle \langle \mathbf{u}_f''' \otimes \mathbf{u}_f''' \otimes \mathbf{u}_f''' \rangle_f + \frac{1}{\rho_f} \nabla \cdot \langle \bar{\boldsymbol{\sigma}}_f \otimes \mathbf{u}_f''' \rangle - \frac{1}{\rho_f} \nabla \langle p_f \mathbf{u}_f''' \rangle \quad (22)$$

347 Finally, the terms left to close are the pressure strain and dissipation terms. These
348 terms are explicitly modelled in the $\overline{v_f^2} - f$ transport equation and are grouped into
349 a source term denoted $k_f f$.

$$k_f f = \underbrace{\phi_{f,yy}}_{\text{pressure strain}} - \underbrace{\varepsilon_{f,yy}}_{\text{dissipation}} + \alpha_f \rho_f 6 \frac{\overline{v_f^2}}{k_f} \varepsilon_f \quad (23)$$

350 The source term effectively redistributes turbulence energy from the stream-wise
351 Reynolds stress component to the wall-normal component close to walls. This is
352 intuitive as previously discussed, when one considers a fully developed turbulent
353 boundary layer as the wall-normal Reynolds stress component's production is zero
354 due to the mean stream-wise flow gradient. This means that turbulence energy can
355 only enter the wall-normal component through redistribution. The source term has
356 been shown to overproduce in regions relatively far away from the wall and the
357 correction of Davidson et al. [6] is employed.

$$\overline{v_{f,source}^2} = \min \left\{ k_f f, -\frac{1}{T} \left[(C_1 - 6) \overline{v_f^2} - \frac{2k_f}{3} (C_1 - 1) \right] + C_2 \Pi_f \right\} \quad (24)$$

358 Now setting the wall-normal component of the fluid-phase Reynolds stress tensor
359 $\langle \mathbf{u}_f''' \otimes \mathbf{u}_f''' \rangle_f$ to v_f^2 a transport equation can be written

$$\frac{\partial(\alpha_f \rho_f \overline{v_f^2})}{\partial t} + \nabla \cdot (\alpha_f \rho_f \overline{v_f^2} \mathbf{u}_f) = \nabla \cdot \left(\mu_f + \frac{\mu_{ft}}{\sigma_{fk}} \right) \nabla \overline{v_f^2} + \alpha_f \rho_f \overline{v_{f,source}^2} - \alpha_f \rho_f 6 \frac{\overline{v_f^2}}{k_f} \varepsilon_f + 2\beta(\overline{v_{fp}^2} - \overline{v_f^2}) \quad (25)$$

360 The reader should note that the third term is a sink term that is used to balance
361 the source term $k_f f$. This is a modification proposed by Lien and Kalitzin [8] and
362 ensures that the source term $k_f f \rightarrow 0$ as it approaches the wall.
363

364 Eq. 25 contains no sensitivity to the wall distance and thus a modified Helmholtz

365 equation is constructed to form an elliptic relaxation equation. The form of this
 366 equation accounts for anisotropy close to walls and is also independent of Reynolds
 367 number and y^+ value which reads

$$L^2 \frac{\partial^2 f}{\partial x^2} - f = \underbrace{\frac{C_1}{T} \left(\frac{\overline{v_f^2}}{k_f} - \frac{2}{3} \right)}_{\phi_{f,yy,S}} - \underbrace{C_2 \frac{\Pi_f}{k_f}}_{\phi_{f,yy,R}} - \frac{1}{T} \left(6 \frac{\overline{v_f^2}}{k_f} - \frac{2}{3} \right) \quad (26)$$

368
 369 The terms $\phi_{f,yy,S}$ and $\phi_{f,yy,R}$ are the so-called slow and rapid pressure-strain terms
 370 [1, 33] with the final term being used to ensure far field behaviour i.e. that the elliptic
 371 relaxation function diminishes away from walls.

372 One drawback of employing a methodology that requires the solution of Poisson's
 373 equation is its elliptic nature. When solving the equation with a segregated solver as
 374 in this work a numerical problem arises as information from upstream is not available.

375 To circumvent these issues Lien and Kalitzin [8] introduced the $6 \frac{\overline{v_f^2}}{k_f}$ as a sink and
 376 source in $k_f f$ source term in the $\overline{v_f^2}$ transport equation. It is also introduced in the
 377 transport equation of f . This ensures that f correctly tends to 0 at a wall allowing a
 378 Dirichlet boundary condition to be prescribed. The eddy viscosity is calculated from
 379 the solution of the $\overline{v_f^2} - f$ model, again the correction proposed by Davidson et al.
 380 [6] is used.

$$\nu_{ft} = \min \left\{ C_{f\mu} k_f^2 / \varepsilon_f, C_\mu \overline{v_f^2} T \right\} \quad (27)$$

381
 382 where the turbulent time and length scales are defined as

$$T = \max \left(\frac{k_f}{\varepsilon_f}, 6 \sqrt{\frac{\nu_f}{\varepsilon_f}} \right) \quad (28)$$

$$L = \max \left(\frac{k_f^{3/2}}{\varepsilon_f}, C_\eta \frac{\nu_f^{3/4}}{\varepsilon_f^{1/4}} \right) \quad (29)$$

383
 384 Both time and length scales are limited in regions close to the wall. This is achieved
 385 by introducing a dependency on Kolmogorov scales which are only active in regions
 386 very close to the wall i.e. $y^+ < 5$. This ensures that a singularity is not introduced
 387 into the solution matrix and that the scales collapse at the wall.

388 **Nomenclature**

C_D	drag coefficient, [-]
Re_p	particle Reynolds number, [-]
d_p	particle diameter, [m]
\mathbf{u}_i	velocity, [ms^{-1}]
p_i	pressure, [Pa]
g_0	radial distribution coefficient, [-]
t	time, [s]
k_i	turbulent kinetic energy, [m^2s^{-2}]

389 *Greek letters*

α_i	volume fraction, [-]
$\alpha_{p,max}$	maximum particle volume fraction, [-]
β	momentum exchange coefficient, [$kgm^{-3}s^{-1}$]
ε_i	turbulent kinetic energy dissipation, [m^2s^{-3}]
Θ_p	granular temperature, [m^2s^{-2}]
κ_p	particle fluctuation energy, [m^2s^{-2}]
κ_{Θ_s}	diffusion coefficient for granular energy, [$kgm^{-1}s^{-1}$]
μ_i	shear viscosity, [$kgm^{-1}s^{-1}$]
$\mu_{i,t}$	turbulent shear viscosity, [$kgm^{-1}s^{-1}$]
ν_i	kinematic viscosity, [m^2s^{-1}]
$\nu_{i,t}$	turbulent kinematic viscosity, [m^2s^{-1}]
ρ_i	density, [kgm^{-3}]
$\bar{\sigma}_f$	fluid phase stress tensor, [$kgm^{-1}s^{-2}$]
$\bar{\sigma}_p$	particle phase stress tensor, [$kgm^{-1}s^{-2}$]
τ_d	particle relaxation time, [s]

390 *Subscripts*

f	fluid
i	general index
p	particle
x	x direction
y	y direction
z	z direction
i, yy	wall normal component w.r.t each phase

391 *Superscripts*

"	PA particle velocity fluctuation
'''	PA fluid velocity fluctuation

392 *Special notation*

$\langle \cdot \rangle$	Reynolds averaging operator
$\langle \cdot \rangle_i$	phase averaging operator associated with phase i

ACCEPTED MANUSCRIPT

Table 3: Model characteristics & turbulence variables.

$$\beta = \frac{\rho_p \alpha_p}{\tau_d} = \frac{3}{4} \frac{\alpha_p \alpha_f \rho_f \mathbf{u}_r}{d_p} C_d$$

$$C_d = \begin{cases} \frac{24}{Re_p} [1 + 0.15 Re_p^{0.287}] & \text{if } Re_p < 1000 \\ 0.44 & \text{if } Re_p \geq 1000 \end{cases}$$

$$u_{p,rms} = \kappa_p = k_p + 3/2 \Theta_p$$

$$St = \tau_d / \tau_f$$

$$\tau_f = k_f / \varepsilon_f$$

$$e = 1$$

$$\Pi_p = 2\nu_{pt} \bar{\mathbf{S}}_p : \bar{\mathbf{S}}_p + \frac{2}{3} k_p \nabla \cdot \mathbf{u}_p$$

$$\Pi_f = 2\nu_{ft} \bar{\mathbf{S}}_f : \bar{\mathbf{S}}_f + \frac{2}{3} k_f \nabla \cdot \mathbf{u}_f$$

$$\varepsilon_f \rightarrow 2\nu_f \frac{k_f}{y^2}$$

$$T = \max\left(\frac{k_f}{\varepsilon_f}, 6 \sqrt{\frac{\nu_f}{\varepsilon_f}}\right)$$

$$L = \max\left(\frac{k_f^{3/2}}{\varepsilon_f}, C_\eta \frac{\nu_f^{3/4}}{\varepsilon_f^{1/4}}\right)$$

$C_{\varepsilon 1}$	$C_{\varepsilon 2}$	C_μ	C_1	C_2	C_L	C_η	β_ϵ	$C_{f\mu}$	$C_{p\mu}$	σ_k	σ_ϵ
1.6	1.9	0.22	1.4	0.3	0.23	70	1	0.09	0.09	1	1

Table 4: Definition of variables.

$$\kappa_p = k_p + 1.5\Theta_p$$

$$\mu_f = \rho_f \nu_f$$

$$\mu_{ft} = \alpha_f \rho_f \nu_{ft} = \alpha_f \rho_f C_\mu \overline{v_f^2} T$$

$$\mu_p = \alpha_p \rho_p \nu_p = \frac{2\mu_{p,dil}}{(1+e)g_0} \left[1 + \frac{4}{5}(1+e)g_0\alpha_p \right]^2 + \frac{4}{5}\alpha_p^2 \rho_p d_p g_0 (1+e) \left(\frac{\Theta_p}{\pi} \right)^{1/2}$$

$$\mu_{p,dil} = \frac{5\sqrt{\pi}}{96} \rho_p d_p \Theta_p^{1/2}$$

$$\mu_{pt} = \alpha_p \rho_p \nu_{pt} = \alpha_p \rho_p C_\mu \overline{v_p^2} T$$

$$p_p = \rho_p \alpha_p \Theta_p + 2(1+e)\rho_p \alpha_p^2 g_0 \Theta_p$$

$$\gamma = \frac{12(1-e^2)g_0}{\sqrt{\pi}d_p} \alpha_p^2 \rho_p \Theta_p^{3/2}$$

$$\kappa_\Theta = \frac{2}{(1+e)g_0} \left[1 + \frac{6}{5}(1+e)g_0\alpha_p \right]^2 \kappa_{\Theta,dil} + 2\alpha_p^2 \rho_p d_p g_0 (1+e) \left(\frac{\Theta_p}{\pi} \right)^{1/2}$$

$$\kappa_{\Theta,dil} = \frac{75}{384} \sqrt{\pi} \rho_p d_p \Theta_p^{1/2}$$

$$g_0 = \left[1 - \left(\frac{\alpha_p}{\alpha_{p,max}} \right)^{\frac{1}{3}} \right]^{-1}$$

$$\overline{\mathbf{S}}_p = \frac{1}{2} [\nabla \mathbf{u}_p + (\nabla \mathbf{u}_p)^T] - \frac{1}{3} \nabla \cdot \mathbf{u}_p \mathbf{I}$$

$$\overline{\mathbf{S}}_f = \frac{1}{2} [\nabla \mathbf{u}_f + (\nabla \mathbf{u}_f)^T] - \frac{1}{3} \nabla \cdot \mathbf{u}_f \mathbf{I}$$

$$k_{fp} = \beta_k \sqrt{k_f k_p}$$

$$\varepsilon_{fp} = \beta_\varepsilon \sqrt{\varepsilon_f \varepsilon_p}$$

$$\overline{v_{fp}^2} = \beta_v \sqrt{v_f^2 v_p^2}$$

Table 5: Definition of phase-averaged variables.

$$\alpha_p = \langle \alpha_p \rangle$$

$$\alpha_f = \langle \alpha_f \rangle$$

$$\mathbf{u}_p = \langle \mathbf{u} \rangle_p$$

$$\mathbf{u}_f = \langle \mathbf{u} \rangle_f$$

$$\Theta_p = \langle \Theta \rangle_p$$

$$k_p = \frac{1}{2} \langle \mathbf{u}_p'' \cdot \mathbf{u}_p'' \rangle_p$$

$$k_f = \frac{1}{2} \langle \mathbf{u}_f''' \cdot \mathbf{u}_f''' \rangle_f$$

$$\varepsilon_p = \frac{1}{\rho_p \alpha_p} \langle \bar{\boldsymbol{\sigma}}_p : \nabla \mathbf{u}_p'' \rangle$$

$$\varepsilon_f = \frac{1}{\rho_f \alpha_f} \langle \bar{\boldsymbol{\sigma}}_f : \nabla \mathbf{u}_f''' \rangle$$

$$\bar{\boldsymbol{\sigma}}_p = \mu_p [\nabla \mathbf{u}_p + (\nabla \mathbf{u}_p)^T] - \frac{1}{3} \mu_p \nabla \cdot \mathbf{u}_p \mathbf{I}$$

$$\bar{\boldsymbol{\sigma}}_f = \mu_f [\nabla \mathbf{u}_f + (\nabla \mathbf{u}_f)^T] - \frac{1}{3} \mu_f \nabla \cdot \mathbf{u}_f \mathbf{I}$$

$$\mathbf{u}_p'' = \mathbf{u}_p - \langle \mathbf{u}_p \rangle_p$$

$$\mathbf{q}_\Theta = \langle \mathbf{q}_\Theta \rangle_p = \frac{\kappa_\Theta}{\alpha_p \rho_p} \nabla \Theta_p$$

$$\mathbf{u}_f''' = \mathbf{u}_f - \langle \mathbf{u}_f \rangle_f$$

$$\langle \mathbf{u}_p \rangle_p = \langle \alpha_p \mathbf{u}_p \rangle / \langle \alpha_p \rangle$$

$$\langle \mathbf{u}_f \rangle_f = \langle \alpha_f \mathbf{u}_f \rangle / \langle \alpha_f \rangle$$

$$\mathbf{u}_p'' \mathbf{u}_p'' = \langle \mathbf{u}_p'' \mathbf{u}_p'' \rangle_p$$

393 **8. Bibliography**394 **References**

- 395 [1] S. B. Pope, *Turbulent flows*. Cambridge: Cambridge Univ. Press, 2011.
- 396 [2] J. C. R. Hunt and J. M. R. Graham, “Free-stream turbulence near plane bound-
397 aries,” *Journal of Fluid Mechanics*, vol. 84, no. 2, pp. 209–235, 1978.
- 398 [3] N. H. Thomas and P. E. Hancock, “Grid turbulence near a moving wall,” *Journal*
399 *of Fluid Mechanics*, vol. 82, no. 3, pp. 481–496, 1977.
- 400 [4] P. A. Durbin, “Near-wall turbulence closure modeling without “damping
401 functions”,” *Theoretical and Computational Fluid Dynamics*, vol. 3, no. 1, pp.
402 1–13, Sep 1991. [Online]. Available: <https://doi.org/10.1007/BF00271513>
- 403 [5] M. Behnia, S. Parneix, and P. Durbin, “Prediction of heat transfer in
404 an axisymmetric turbulent jet impinging on a flat plate,” *International*
405 *Journal of Heat and Mass Transfer*, vol. 41, no. 12, pp. 1845 – 1855,
406 1998. [Online]. Available: <http://www.sciencedirect.com/science/article/pii/S0017931097002548>
407
- 408 [6] L. Davidson, P. V. Nielsen, and A. Sveningsson, “Modifications of the v2-f model
409 for computing the flow in a 3d wall jet,” in *Turbulence, heat and mass transfer*,
410 K. Hanjalić, Y. Nagano, and M. Tummers, Eds., 2003, pp. 577–584.
- 411 [7] P. A. Durbin and B. A. P. Reif, *Statistical theory and modeling of turbulence*
412 *flow*. John Wiley & Sons, Ltd, 2010, pp. 109–154. [Online]. Available:
413 <http://dx.doi.org/10.1002/9780470972076.ch6>
- 414 [8] F.-S. Lien and G. Kalitzin, “Computations of transonic flow with
415 the v2-f turbulence model,” *International Journal of Heat and Fluid*
416 *Flow*, vol. 22, no. 1, pp. 53–61, 2001. [Online]. Available: <http://www.sciencedirect.com/science/article/pii/S0142727X00000734>
417
- 418 [9] A. Sveningsson, “Analysis of the Performance of Different v2f Turbulence Models
419 in a Stator Vane Passage Flow,” Ph.D. dissertation, Chalmers University of
420 Technology, 2003.
- 421 [10] M. A. Rizk and S. E. Elghobashi, “A two-equation turbulence model for dis-
422 persed dilute confined two-phase flows,” *International Journal of Multiphase*
423 *Flow*, vol. 15, no. 1, pp. 119–133, 1989.

- 424 [11] B. Vreman, B. J. Geurts, N. G. Deen, J. A. M. Kuipers, and
425 J. G. M. Kuerten, “Two- and four-way coupled euler-lagrangian large-eddy
426 simulation of turbulent particle-laden channel flow,” *Flow, Turbulence and*
427 *Combustion*, vol. 82, no. 1, pp. 47–71, Jan 2009. [Online]. Available:
428 <https://doi.org/10.1007/s10494-008-9173-z>
- 429 [12] S. Benyahia, M. Syamlal, and T. J. O’Brien, “Evaluation of boundary conditions
430 used to model dilute, turbulent gas/solids flows in a pipe,” *Powder Technology*,
431 vol. 156, no. 2, pp. 62 – 72, 2005, particle Technology Forum Special
432 Issue. [Online]. Available: <http://www.sciencedirect.com/science/article/pii/S0032591005001245>
433
- 434 [13] A. Benavides and B. van Wachem, “Numerical simulation and validation of
435 dilute turbulent gas-particle flow with inelastic collisions and turbulence modu-
436 lation,” *Powder Technology*, vol. 182, pp. 294–306, 2008.
- 437 [14] S. Dasgupta, R. Jackson, and S. Sundaresan, “Turbulent gas-particle flow in
438 vertical risers,” *AIChE Journal*, vol. 40, no. 2, pp. 215–228, 1994. [Online].
439 Available: <http://dx.doi.org/10.1002/aic.690400204>
- 440 [15] Y. Reinhardt and L. Kleiser, “Validation of Particle-Laden Turbulent Flow Sim-
441 ulations Including Turbulence Modulation,” *Journal of Fluids Engineering*, vol.
442 137, no. 7, p. 71303, 2015.
- 443 [16] M. T. Shah, R. P. Utikar, V. K. Pareek, M. O. Tade, and G. M. Evans,
444 “Effect of closure models on eulerian-eulerian gas-solid flow predictions in
445 riser,” *Powder Technology*, vol. 269, pp. 247 – 258, 2015. [Online]. Available:
446 <http://www.sciencedirect.com/science/article/pii/S0032591014007785>
- 447 [17] T. Strömngren, G. Brethouwer, G. Amberg, and A. V. Johansson, “Modelling
448 of turbulent gas-particle flows with focus on two-way coupling effects on
449 turbophoresis,” *Powder Technology*, vol. 224, pp. 36–45, 2012. [Online].
450 Available: <http://dx.doi.org/10.1016/j.powtec.2012.02.017>
- 451 [18] E. J. Bolio, J. A. Yasuna, and J. L. Sinclair, “Dilute turbulent gas-solid flow
452 in risers with particle-particle interactions,” *AIChE Journal*, vol. 41, no. 6, pp.
453 1375–1388, 1995.
- 454 [19] S. Dasgupta, R. Jackson, and S. Sundaresan, “Gas-particle flow in vertical
455 pipes with high mass loading of particles,” *Powder Technology*, vol. 96, no. 1,

- 456 pp. 6 – 23, 1998. [Online]. Available: [http://www.sciencedirect.com/science/](http://www.sciencedirect.com/science/article/pii/S0032591097033482)
457 [article/pii/S0032591097033482](http://www.sciencedirect.com/science/article/pii/S0032591097033482)
- 458 [20] Y. Zheng, X. Wan, Z. Qian, F. Wei, and Y. Jin, “Numerical simulation of the
459 gas-particle turbulent flow in riser reactor based on $k-\epsilon-kp-\epsilon p-\theta$ two-fluid model,”
460 *Chemical Engineering Science*, vol. 56, no. 24, pp. 6813–6822, 2001.
- 461 [21] V. C. Patel, W. Rodi, and G. Scheuerer, “Turbulence models for near-wall and
462 low Reynolds number flows - A review,” *AIAA Journal*, vol. 23, no. 9, pp. 1308–
463 1319, 1985. [Online]. Available: <http://arc.aiaa.org/doi/abs/10.2514/3.9086>
- 464 [22] M. Reeks, “The transport of discrete particles in inhomogeneous turbulence,”
465 *Journal of Aerosol Science*, vol. 14, no. 6, pp. 729 – 739, 1983. [Online]. Available:
466 <http://www.sciencedirect.com/science/article/pii/0021850283900551>
- 467 [23] Y. Yamamoto, M. Potthoff, T. Tanaka, T. Kajishima, and Y. Tsuji, “Large-
468 eddy simulation of turbulent gas-particle flow in a vertical channel: effect of
469 considering inter-particle collisions,” *Journal of Fluid Mechanics*, vol. 442, pp.
470 303–334, 2001.
- 471 [24] P. Fevrier, O. Simonin, and K. D. Squires, “Partitioning of particle velocities
472 in gas solid turbulent flows into a continuous field and a spatially uncorrelated
473 random distribution: theoretical formalism and numerical study,” *Journal of*
474 *Fluid Mechanics*, vol. 533, pp. 1–46, 2005.
- 475 [25] R. O. Fox, “On multiphase turbulence models for collisional fluid-particle flows,”
476 *Journal of Fluid Mechanics*, vol. 742, pp. 368–424, 2014.
- 477 [26] M. Riella, R. Kahraman, and G. Tabor, “Reynolds-averaged two-fluid model
478 prediction of moderately dilute fluid-particle flow over a backward-facing
479 step,” *International Journal of Multiphase Flow*, vol. 106, pp. 95 – 108,
480 2018. [Online]. Available: [https://www.sciencedirect.com/science/article/pii/](https://www.sciencedirect.com/science/article/pii/S0301932217309850)
481 [S0301932217309850](https://www.sciencedirect.com/science/article/pii/S0301932217309850)
- 482 [27] E. Peirano and B. Leckner, “Fundamentals of turbulent gas-solid flows applied
483 to circulating fluidized bed combustion,” *Doktorsavhandlingar vid Chalmers*
484 *Tekniska Hogskola*, vol. 24, no. 1381, pp. 259–296, 1998.
- 485 [28] C. Marchioli, A. Soldati, J. Kuerten, B. Arcen, A. Tanière, G. Goldensoph,
486 K. Squires, M. Cargnelutti, and L. Portela, “Statistics of particle dispersion
487 in direct numerical simulations of wall-bounded turbulence: Results of

- 488 an international collaborative benchmark test,” *International Journal of*
489 *Multiphase Flow*, vol. 34, no. 9, pp. 879 – 893, 2008. [Online]. Available:
490 <http://www.sciencedirect.com/science/article/pii/S0301932208000414>
- 491 [29] M. Riella, “Turbulence modelling of fluid-particle interaction,” Ph.D. disserta-
492 tion, University of Exeter, 2019.
- 493 [30] M. Syamlal and T. J. O’Brien, “Computer simulation of bubbles in a fluidized
494 bed,” *AIChE Symposium Series*, vol. 85, no. 270, pp. 22–31, 1989.
- 495 [31] B. G. M. Van Wachem, J. C. Schouten, C. M. Van den Bleek, R. Krishna, and
496 J. L. Sinclair, “Comparative analysis of CFD models of dense gas-solid systems,”
497 *AIChE Journal*, no. 5, 2001.
- 498 [32] J. Capecelatro, O. Desjardins, and R. O. Fox, “On fluid-particle dynamics in
499 fully developed cluster-induced turbulence,” *Journal of Fluid Mechanics*, vol.
500 780, pp. 578–635, 2015.
- 501 [33] B. E. Launder, G. J. Reece, and W. Rodi, “Progress in the development of a
502 reynolds-stress turbulence closure,” *Journal of Fluid Mechanics*, vol. 68, no. 3,
503 pp. 537–566, 1975.
- 504 [34] H. G. Weller, G. Tabor, H. Jasak, and C. Fureby, “A tensorial approach to com-
505 putational continuum mechanics using object-oriented techniques,” *Computers*
506 *in Physics*, vol. 12, no. 6, pp. 620–631, 1998.
- 507 [35] J. H. Ferziger and M. Peric, *Computational Methods for Fluid Dynamics*.
508 Springer, 2002.
- 509 [36] R. I. Issa, “Solution of the implicitly discretised fluid flow equations by operator-
510 splitting,” *Journal of Computational Physics*, vol. 62, no. 1, pp. 40–65, 1986.
- 511 [37] S. T. Zalesak, “Fully multidimensional flux-corrected transport algorithms for
512 fluids,” *Journal of Computational Physics*, vol. 31, no. 3, pp. 335–362, 1979.
- 513 [38] A. W. Vreman, “Turbulence attenuation in particle-laden flow in smooth and
514 rough channels,” *Journal of Fluid Mechanics*, vol. 773, pp. 103–136, 2015.
- 515 [39] M. W. Vance, K. D. Squires, and O. Simonin, “Properties of the particle velocity
516 field in gas-solid turbulent channel flow,” *Physics of Fluids*, vol. 18, no. 6, p.
517 063302, 2006.

- 518 [40] C. Marchioli and A. Soldati, “Mechanisms for particle transfer and segregation in
519 a turbulent boundary layer,” *Journal of Fluid Mechanics*, vol. 468, pp. 283–315,
520 2002.
- 521 [41] M. Riella, “ratfmfoam: A reynolds-averaged two-fluid solver for openfoam-
522 2.2.2.” dec 2018, <https://github.com/mjriella/ratfmFoam>. [Online]. Available:
523 <https://doi.org/10.5281/zenodo.2301515>

ACCEPTED MANUSCRIPT